FEBS Letters 587 (2013) 2232–2240

journal homepage: www.FEBSLetters.org

Functional evaluation of Asp76, 84, 102 and 150 in human arsenic(III) methyltransferase (hAS3MT) interacting with S-adenosylmethionine

Xiangli Li [a], Zhirong Geng [a,*], Shuping Wang [a], Xiaoli Song [b], Xin Hu [c], Zhilin Wang [a,*]

[a] State Key Laboratory of Coordination Chemistry, School of Chemistry and Chemical Engineering, Nanjing University, Nanjing 210093, PR China
[b] School of Chemistry and Chemical Engineering, Yangzhou University, Yangzhou 225002, PR China
[c] Modern Analysis Center of Nanjing University, Nanjing 210093, PR China

ARTICLE INFO

Article history:
Received 2 May 2013
Revised 23 May 2013
Accepted 23 May 2013
Available online 4 June 2013

Edited by Peter Brzezinski

Keywords:
Human arsenic(III) methyltransferase (hAS3MT)
Mutants
S-adenosylmethionine
Hydrogen bond

ABSTRACT

We prepared eight mutants (D76P, D76N, D84P, D84N, D102P, D102N, D150P and D150N) to investigate the functions of residues Asp76, 84, 102 and 150 in human arsenic(III) methyltransferase (hAS3MT) interacting with the S-adenosylmethionine (SAM)-binding. The affinity of all the mutants for SAM were weakened. All the mutants except for D150N completely lost their methylation activities. Residues Asp76, 84, 102 and 150 greatly influenced hAS3MT catalytic activity via affecting SAM-binding or methyl transfer. Asp76 and 84 were located in the SAM-binding pocket, and Asp102 significantly affected SAM-binding via forming hydrogen bonds with SAM.

1. Introduction

S-adenosylmethionine (SAM) is recognized as the major methyl donor of methylation reactions catalyzed by methyltransferase [1–3]. The methylation of lipids, proteins, DNA and other small molecules (inorganic arsenic, chloride, bromide) significantly affect many important biological processes including biosynthesis, protein repair, signal transduction, metabolism and detoxification [4–7]. The methylation of inorganic arsenic (iAs) has been well known as the main arsenic metabolic process, the mechanism of which has been studied for many years [8,9]. Arsenic(III) methyltransferase (AS3MT) catalyzes the biotransformation of iAs, which needs a reductant and SAM as the enzyme cofactors [10–12]. Investigating SAM-binding sites and As-binding sites in AS3MT helps to understand the methyl transfer process, which further assists to elucidate the mechanism of the arsenic methylation. The active sites and As-binding sites in AS3MT have been studied previously. Residues Cys157 and Cys207 in recombinant mouse AS3MT and Cys156 in rat AS3MT have been demonstrated to be the As-binding sites and active sites, respectively [13,14]. Cys156 and Cys206 in human AS3MT (hAS3MT) are also the As-binding sites [15]. However, the binding sites of cofactor SAM in hAS3MT are still undefined.

Several sequence motifs in hAS3MT proteins have been predicted to interact with SAM via multiple-sequence alignments resembling many SAM-dependent methyltransferases [1,16,17]. The motif I of hAS3MT is the 74-ILDLGSGSG-82 sequence conformed to the general consensus motif I (hh (D/E) hGXGXG), where h is a hydrophobic amino acid, X is any amino acid, and residues D and G (glycine residues) are strongly conserved. The motif II is 101-IDMT-104, which contains a conserved acidic residue Asp102. The sequences of motif III are 147-ESHDIVVSN-155 with an invariant Asp150 at position 4. However, the actual functions of the residues in the motifs mentioned above have not been clarified by experiments.

To better understand the mechanisms of arsenic methylation and the methyl transfer from SAM to As, SAM-binding sites in hAS3MT need to be investigated in detail. Thereby motivated, we herein first studied the functions of acidic residues Asp76, 84, 102 and 150 in the motifs or near the motif of hAS3MT because the acidic residues with carboxyl groups in other SAM-dependent

Abbreviations: iAs, inorganic arsenic; MMA, monomethylated arsenicals; DMA, dimethylated arsenicals; AS3MT, arsenic(III) methyltransferase; SAM, S-adenosylmethionine; GSH, glutathione; CD, circular dichroism; BSA, bovine serum albumin; isopropyl, β-D-thiogalactopyranoside (IPTG); ATR-FTIR, attenuated total reflection Fourier transform infrared spectrometry; WT, wild-type; HPLC-ICP-MS, high performance liquid chromatography-inductively coupled plasma-mass spectrometry; SDS–PAGE, sodium dodecyl sulfate–polyacrylamide gel electrophoresis; CmArsM, cyanidioschyzon merolae arsenite S-adenosylmethyltransferase

* Corresponding authors. Fax: +86 25 83317761.
E-mail addresses: gengzr@nju.edu.cn (Z. Geng), wangzl@nju.edu.cn (Z. Wang).

0014-5793/$36.00
http://dx.doi.org/10.1016/j.febslet.2013.05.052

Table 1
Primers used for site-directed mutagenesis.

	Primer	Sequence
D76P	+	5′ CACTACCCAG**CGG**CAAAATCC 3′
	–	5′AACTGCTGGATTTTG**CCG**CTGGG3′
D76N	+	5′ CACTACCCAG**ATT**CAAAATCC 3′
	–	5′AACTGCTGGATTTTG**AAT**CTGGG3′
D84P	+	5′ GGCTAAGTACATAGCA**CGG**TCTACC 3′
	–	5′ GGTAGA**CCG**TGCTATGTACTTAGCC 3′
D84N	+	5′ GGCTAAGTACATAGCA**ATT**TCTACC 3′
	–	5′ GGTAGA**AAT**TGCTATGTACTTAGCC 3′
D102P	+	5′ TTGGTCAT**CGG**TATTCCAGTCACGT 3′
	–	5′ GACACGTGACTGGAATA**CCG**ATGACC 3′
D102N	+	5′ TTGGTCAT**ATT**TATTCCAGTCACGT 3′
	–	5′ GACACGTGACTGGAATA**AAT**ATGACC 3′
D150P	+	5′ CACAGTTTGATACAACAAT**CGG**ATGG 3′
	–	5′ GAATGAGAGCCAT**CCG**ATTG 3′
D150N	+	5′ CACAGTTTGATACAACAAT**ATT**ATGG 3′
	–	5′ GAATGAGAGCCAT**AAT**ATTG 3′
Whole	+	5′CGGGATATCATGGCTGCACTTCGTGAC3′
	–	5′CGGGTCGACTTAGTGATGGTGATG3′

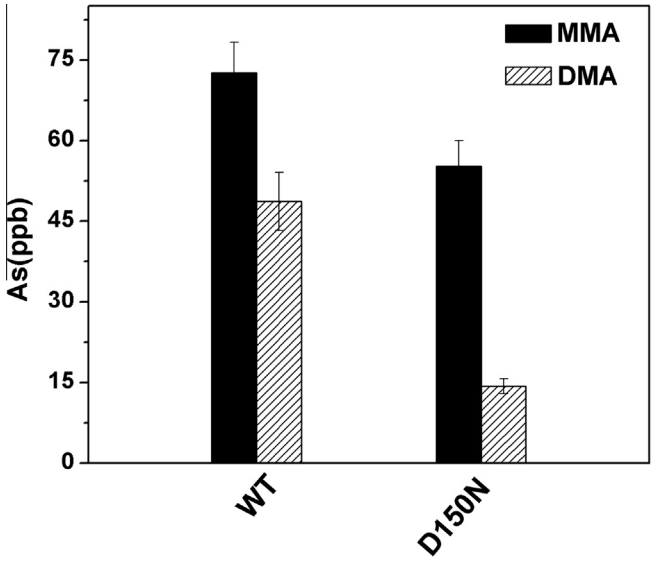

Fig. 1. Catalytic capacity of the hAS3MT mutant. Reaction mixtures (100 μl) containing 11 μg enzymes, 5 μM iAs^{3+}, 1 mM SAM, 7 mM GSH in PBS (25 mM, pH 7.0) were cultured at 37 °C for 2 h. The proportion of methylated arsenic (MMA and DMA) for WT-hAS3MT and only one active mutant D150N were showed. Values are the means ± S.D. of three independent experiments.

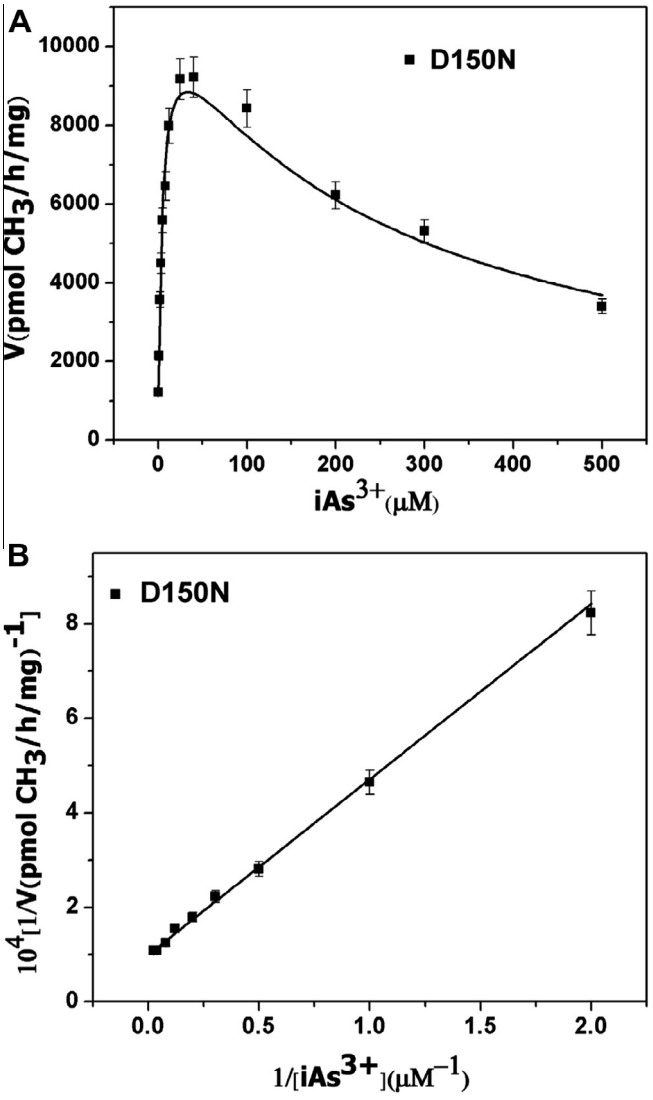

Fig. 2. (A) Substrate concentration dependence of rate for the mutant D150N. The line show the least squares fit of Eq. (1) to the data. (B) Double reciprocal plot of the arsenic methylation rate against the concentration of iAs^{3+} for the mutant D150N. Reaction mixtures (100 μl) containing 11 μg D150N, 1 mM SAM, 7 mM GSH and 0.5–500 μM iAs^{3+} in PBS (25 mM, pH 7.0) were incubated at 37 °C for 2 h. Values are the means ± S.D. of three independent experiments.

methyltransferases have been confirmed to play important roles in SAM binding via forming hydrogen bonds with SAM directly or through water molecules [18–21]. Based on the previous study, Asp60 in DNA (cystosine-5) methyltransferases was replaced by residue Pro and Asn [22]. Thus eight mutants D76P, D76N, D84P, D84N, D102P, D102N, D150P and D150N in hAS3MT were obtained by site-directed mutagenesis. Their catalytic activities and conformations were determined and the models of the hAS3MT-SAM were built by modeller9v8 utilizing the most updated protein template Cyanidioschyzon merolae arsenite S-adenosylmethyltransferase (CmArsM) (PDB code 4FR0), because both of the hAS3MT and CmArsM were the arsenic methyltransferases existed in different species and their sequences were most similar to each other. We concluded that Asp102 significantly affected the SAM-binding via forming hydrogen bonds with the ribose hydroxyl groups of SAM as well as Asp76 and 84 in the SAM-binding pocket. Besides, using Pro or Asn to substitute the Asp150 also influenced the SAM-binding and enzyme activity via changing the conformation of the enzyme and the microenvironment of the SAM-binding pocket.

2. Materials and methods

Caution: Arsenical compounds are known as human carcinogens and should be handled accordingly [23].

2.1. Materials

The expression host, *Escherichia coli* BL21 (DE3) pLysS, was bought from Novagen. The restriction enzymes, dNTPs and PrimerSTAR HS DNA polymerase, were obtained from Takara. SAM, glutathione (GSH), isopropyl β-D-thiogalactopyranoside (IPTG) and bovine serum albumin (BSA) were purchased from Sigma. Arsenicals were bought from J&K Chemical Ltd.

2.2. Preparation of hAS3MT mutants

The plasmid pET-32a-*hAS3MT* was subjected to the site-directed mutagenesis of *hAS3MT* [15,24]. The primers used for site-directed mutagenesis are summarized in Table 1. After sequencing

Table 2
Kinetic parameters for iAs methylation catalyzed by the mutant D150N.

	[a]V_{max} (pmol CH_3/mg/h)	[a]K_M (μM)	K_I (mM)	[b]V_{max} (pmol CH_3/mg/h)	[b]K_M (μM)	[c]K_M (μM)	Relative [c]K_M
D150N	11222 ± 569	4.4 ± 0.4	0.2 ± 0.03	10055 ± 969	3.74 ± 0.3	245.1 ± 17.6	5.1
WT	21170 ± 1,079	3.2 ± 0.24	0.7 ± 0.09	19836 ± 919	3.19 ± 0.7	47.84	1.0

Values represent the mean ± S.D. of three independent experiments.
[a] Represents the kinetic parameters of iAs^{3+} estimated from the data in Fig. 2A by Eq. (1).
[b] Represents the kinetic parameters of iAs^{3+} calculated from the data in Fig. 2B.
[c] Represent the K_M for SAM.

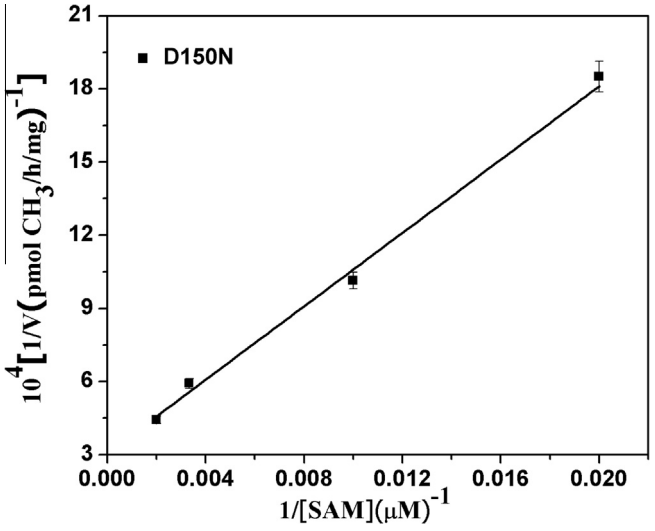

Fig. 3. Double reciprocal plot of the arsenic methylation rate against the concentration of SAM for the mutant D150N. Reaction mixtures (100 μl) containing 11 μg D150N, 5 μM iAs^{3+}, 7 mM GSH and 0.05–2 mM SAM in PBS (25 mM, pH 7.0) were incubated for 2 h at 37 °C. Values are the means ± S.D. of three independent experiments.

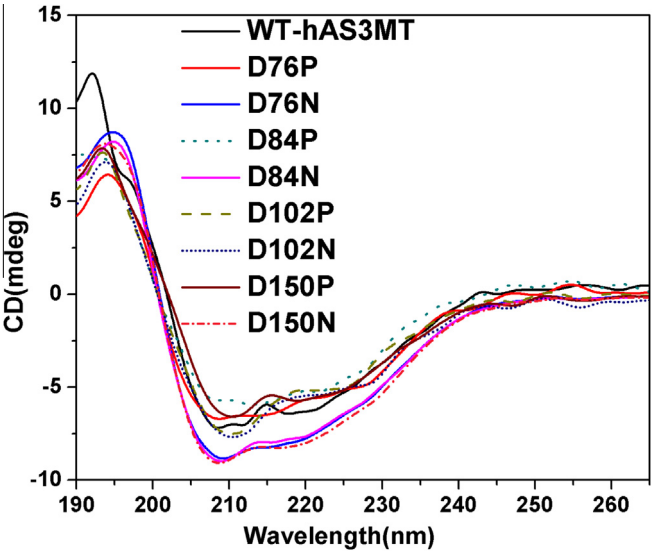

Fig. 4. CD spectra of hAS3MT and the mutants. The spectra were recorded at the protein concentration of 2 μM at room temperature. The plot is the representative of three independent measurements.

[25], the vectors carrying mutant hAS3MT genes were transformed into *E. coli* BL21 (DE3) pLysS for expression. Protein expression and purification were performed following the protocols described previously [24]. All proteins were dialyzed against PBS (25 mM, pH 7.0) at 4 °C to remove imidazole and excess salts. Protein concentrations were determined by the method of Bradford based on a BSA standard curve [26].

Table 3A
Secondary structures of WT-hAS3MT and the mutants estimated from CD spectra.

	α-Helix (%)	β-Pleated (%)	β-Turn (%)	Random (%)
D76P	29.1 ± 1.1	24.0 ± 1.1	16.9 ± 0.9	30.0 ± 0.2
D76N	25.9 ± 0.8	31.6 ± 1.4	14.5 ± 0.3	28.0 ± 1.2
D84P	23.7 ± 1.6	42.6 ± 1.3	6.1 ± 0.8	27.8 ± 0.5
D84N	25.1 ± 1.3	31.0 ± 1.6	15.0 ± 0.6	28.9 ± 1.4
D102P	25.6 ± 0.3	34.0 ± 2.0	12.0 ± 0.9	28.4 ± 0.8
D102N	28.4 ± 1.2	24.8 ± 0.8	15.9 ± 1.0	31.2 ± 0.3
D150P	34.7 ± 1.0	13.5 ± 2.9	20.9 ± 1.2	31.0 ± 0.7
D150N	27.1 ± 1.2	25.5 ± 1.5	17.3 ± 0.8	30.1 ± 1.9
WT	29.0 ± 2.2	23.9 ± 1.9	17.9 ± 1.7	29.2 ± 1.4

The values represent the mean ± S.D. of three independent experiments. The parameters were analyzed with the Jasco secondary structure manager with the reference CD data-Yang. jwr in PBS (25 mM, pH 7.0) at room temperature.

2.3. Enzyme activity assays

The methylation capacity of the mutants was determined in a system (100 μl) containing 11 μg enzyme, 7 mM GSH, 5 μM iAs^{3+} and 1 mM SAM in PBS (25 mM, pH 7.0) [15,24] incubated at 37 °C for 2 h and terminated by adding H_2O_2 to a final concentration of 3%. To measure the iAs^{3+} substrate kinetics, 11 μg enzyme, 7 mM GSH, 1 mM SAM and 0.5–500 μM iAs^{3+} were used. In SAM kinetic experiments, 0.05–2 mM SAM were used and the concentration of other components in the reaction system was without change. The samples were separated by HPLC using an anion-exchange column (PRP X-100 250 × 4.6 mm i.d., 5 μm, Hamilton) and then quantified by ICP-MS (Elan 9000, Perkin–Elmer) with the flow rate of 1.0 ml/min at room temperature [24,27]. The arsenical compounds were eluted with the mobile phase of 15 mM $(NH_4)_2HPO_4$ (pH 6.0). The amounts of arsenic species were calculated with the working curves prepared using 5, 10, 20, 40 and 80 μg/l of standard arsenic species. The methylation rates were calculated as mole equivalents of methyl groups that were transferred from SAM to iAs^{3+} (i.e., 1 nmol CH_3 per 1 nmol monomethylated arsenicals (MMA) or 2 nmol CH_3 per 1 nmol dimethylated arsenicals (DMA)) [28]. The rate of methylation reaction follows the non-competitive substrate inhibition Eq. (1):

$$V = [S] \times V_{max}/(K_M + [S] + [S]^2/K_I) \quad (1)$$

and double reciprocal Eq. (2):

$$1/V = K_M/(V_{max} \times [S]) + 1/V_{max} \quad (2)$$

[15], where V is the initial velocity of the reaction (pmol CH_3 transferred/h/mg protein); $[S]$, the substrate (iAs^{3+}) concentration (μM); V_{max}, the maximal velocity of the reaction (pmol CH_3 transferred/h/mg protein); K_M, the Michaelis constant for iAs^{3+} (μM) and K_I, the inhibition constant for iAs^{3+} (μM).

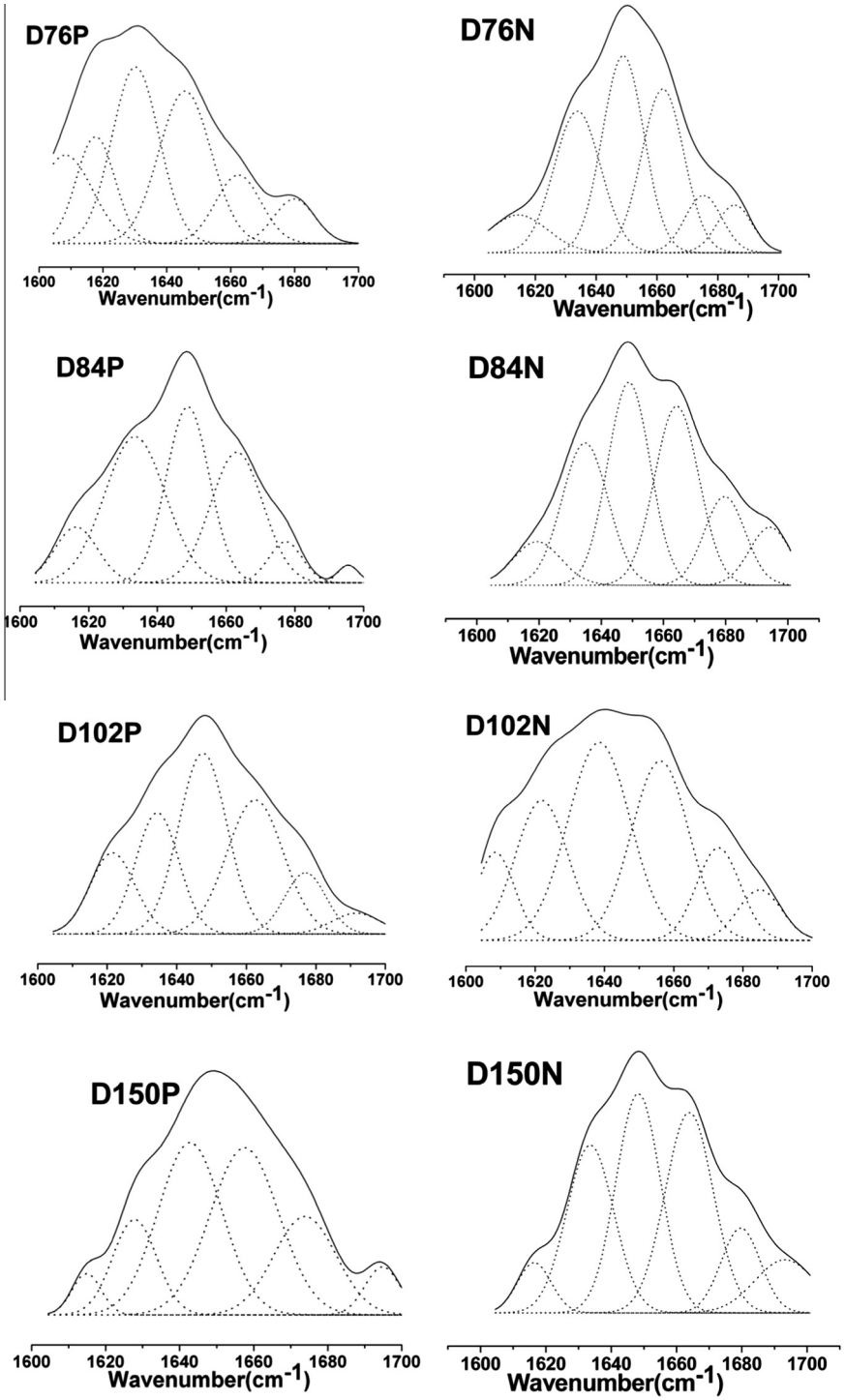

Fig. 5. Curve-fitted amide I region of the mutants. The component peaks are the result of curve-fitting using a Gaussian shape. The solid lines represent the experimental FTIR spectra after Savitzky–Golay smoothing; the dashed lines represent the fitted components. The plot is the representative of three independent measurements.

2.4. CD and ATR-FTIR spectra

Circular dichroism (CD) studies on the WT and hAS3MT mutants were carried out with a JASCO-J810 spectropolarimeter (Jasco Co., Japan) in a 1 mm cell and 10 mm light length at the scanning rate of 50 nm/min. Each spectrum represents the average of three accumulations recorded between 190- and 265-nm of every dilute enzyme solutions (2 μM in 25 mM PBS, pH 7.0) at room temperature with baseline correction. The secondary structure parameters of the mutants were calculated using Jwsse32 software with reference CD-Yang. jwr [29]. Attenuated total reflection Fourier transform infrared spectrometry (ATR-FTIR) spectra were also used to analyze the secondary structures of the mutants. More details about the ATR-FTIR spectra were described in earlier studies [15,16,30].

2.5. Fluorescence spectra

The fluorescence quenching mechanisms of the hAS3MT mutants with increasing SAM concentration were studied [31] by titrating successive additions of a 100 mM SAM stock solution into 2 μM hAS3MT. The fluorescence spectra were measured with a

Table 3B
Secondary structures of WT-hAS3MT and the mutants estimated from ATR-FTIR spectra.

	α-Helix (%)	β-Pleated (%)	β-Turn (%)	Random (%)
D76P	27.3 ± 0.5	25.8 ± 0.3	16.8 ± 0.3	29.9 ± 0.8
D76N	25.2 ± 1.8	31.0 ± 2.3	13.9 ± 0.6	29.9 ± 0.8
D84P	25.8 ± 1.0	40.6 ± 0.4	6.0 ± 0.3	27.5 ± 0.3
D84N	25.8 ± 1.2	27.9 ± 0.8	18.3 ± 0.9	28.0 ± 1.4
D102P	26.5 ± 1.7	30.9 ± 2.5	12.1 ± 1.7	30.5 ± 1.1
D102N	28.1 ± 0.8	24.9 ± 1.3	15.8 ± 0.3	31.2 ± 0.5
D150P	32.3 ± 1.8	15.2 ± 1.7	21.6 ± 0.9	30.9 ± 0.6
D150N	27.8 ± 1.6	27.5 ± 2.1	16.9 ± 1.3	27.8 ± 1.4
WT	26.6 ± 3.6	20.7 ± 4.6	24.2 ± 3.2	28.5 ± 4.9

The values represent the mean ± S.D. of three independent experiments.

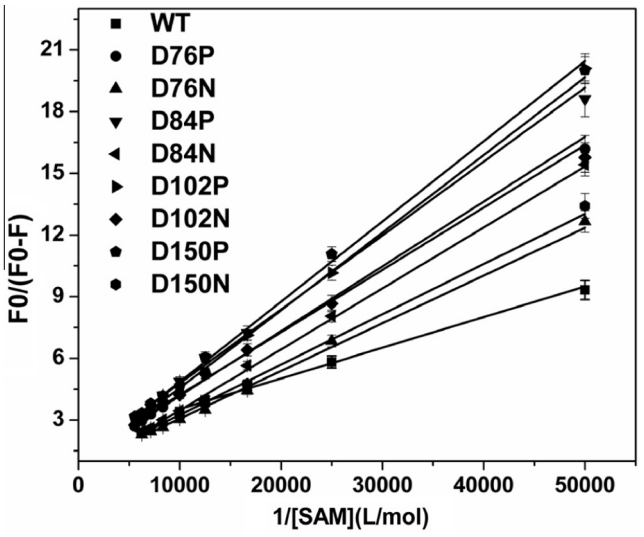

Fig. 6. Plot of $F_0/(F_0 - F)$ versus $[SAM]^{-1}$ of WT and the mutants hAS3MT according to Eq. (3), from which the dissociation constants k_d can be obtained.

Table 4
Dissociation constant k_d and relative k_d of WT and mutants hAS3MT determined at 27 °C.

	k_d (μM)	Relative k_d	R^2
WT	72.5 ± 4.3	1.0	0.99107
D76P	306.2 ± 15.4	4.2	0.99074
D76N	310.5 ± 10.8	4.3	0.99169
D84P	300.8 ± 9.7	4.1	0.9908
D84N	583.7 ± 18.3	8.1	0.99317
D102P	479.1 ± 17.2	6.6	0.99329
D102N	253.9 ± 9.3	3.5	0.99153
D150P	406.8 ± 11.6	5.6	0.99488
D150N	305.5 ± 19.8	4.2	0.99689

48 000 DSCF time-resolved fluorescence spectrometer (SLM Co., USA) and recorded between 300 and 420 nm at 27 °C (excitation at 282 nm). The spectral data obtained were fitted to the equation:

$$F_0/(F_0 - F) = k_d/(f \times [Q]) + 1/f \quad (3)$$

where F_0 and F represents the fluorescence intensities of the enzyme in the absence and presence of cofactor SAM, respectively, $[Q]$ is the concentration of SAM, f is the fractional number of the fluorophores accessible to the quencher SAM and the dissociated constant k_d was calculated graphically from the plot of $F_0/(F_0 - F)$ versus $[Q]^{-1}$ [22,31].

2.6. Modeling of WT-hAS3MT and its mutants using modeller9v8

Using the SAM-CmArsM (PDB code 4FR0) structure as the template [21], models of WT-hAS3MT and hAS3MT mutants with SAM were built with modeller9v8 for the protein sequence of CmArsM is most similar to that of hAS3MT. The models quality of hAS3MT was estimated via QMEAN Server [32]. Chimera 1.5 was used to analyze the models of hAS3MT.

3. Results

3.1. Catalytic activities of the mutants

All the mutants except for D150N lost their catalytic activity completely. The proportion of MMA and DMA for only one active mutant D150N reduced compared to that of WT showed in Fig. 1, which suggested that the catalytic capacity of D150N also turned weaker than that of WT. Thus we concluded that the residues Asp76, 84, 102 and 150 affected the activity of hAS3MT significantly.

Substrate inhibition of rate by iAs^{3+} was observed for D150N in wide iAs^{3+} concentration range (0.5–500 μM) (Fig. 2). The kinetic constants of the active mutant D150N were estimated by fitting Eq. (1) and calculated by double reciprocal plots from Eq. (2) shown in Table 2. The two methods give the consistent results. The K_I values for iAs^{3+} of the mutant D150N was decreased compared to that of WT-hAS3MT (K_M, 3.2 μM; K_I, 0.7 mM; V_{max}, 19,836 pmol/h/mg [15]). The V_{max} values of D150N decreased to 53% of that of WT-hAS3MT. The $K_{M(As)}$ values of D150N was slightly higher than that of WT. The results indicated that the affinity of the mutant D150N to iAs decreased mildly compared to that of WT.

The $K_{M(SAM)}$ value of the mutant D150N reflecting the ability of SAM to interact with hAS3MT, which was calculated from the double reciprocal plot (Fig. 3), was summarized in Table 2. The $K_{M(SAM)}$ value of the mutant D150N increased to 245.1 μM, which was 5.1 folds of WT value (WT: 47.84 μM [15,33]). The data revealed that the residue Asp150 is involved in the cofactor SAM binding, which was the most dominative reason for the catalytic activity of D150N decreased.

3.2. Conformations of the mutants and WT-hAS3MT

The CD spectra of the eight mutants and WT-hAS3MT (Fig. 4) showed that the intensities of the peaks (208 and 220 nm) of mutants D76P, D84P and D102P were lower than those of the wild type enzyme, but those of mutants D76N, D84N, D102P, D102N and D150N were higher. Compared to WT-hAS3MT, the peaks (208 nm) of D102P, D102N and D84P, D150P shifted bathochromically by 2 and 4 nm, respectively. The results aforementioned suggested that the conformations of the eight mutants differed from that of WT. The secondary structures were computed by Jwsse32 software with reference CD-Yang. jwr (Table 3A). The secondary structures of mutants D76P, D102N and D150N were similar to those of WT-hAS3MT while those of mutants D76N, D84N, D84P, D102P and D150P differed significantly from those of WT. Compared with WT, the contents of α-helix, β-pleated sheet and random coil in mutants D76N, D84P, D84N and D102P decreased while that of β-turn increased. Besides, the contents of α-helix, β-pleated sheet and random coil in mutant D150P increased while that of β-turn decreased remarkably.

To further confirm the secondary structures of the mutants, we performed ATR-FTIR assays and analyzed their amide I bands spectrum. The original and curve-fitting FTIR spectra of the mutants were showed in Fig. 5. There are six component bands in the amide I bands of the mutants. According to the well-established assign-

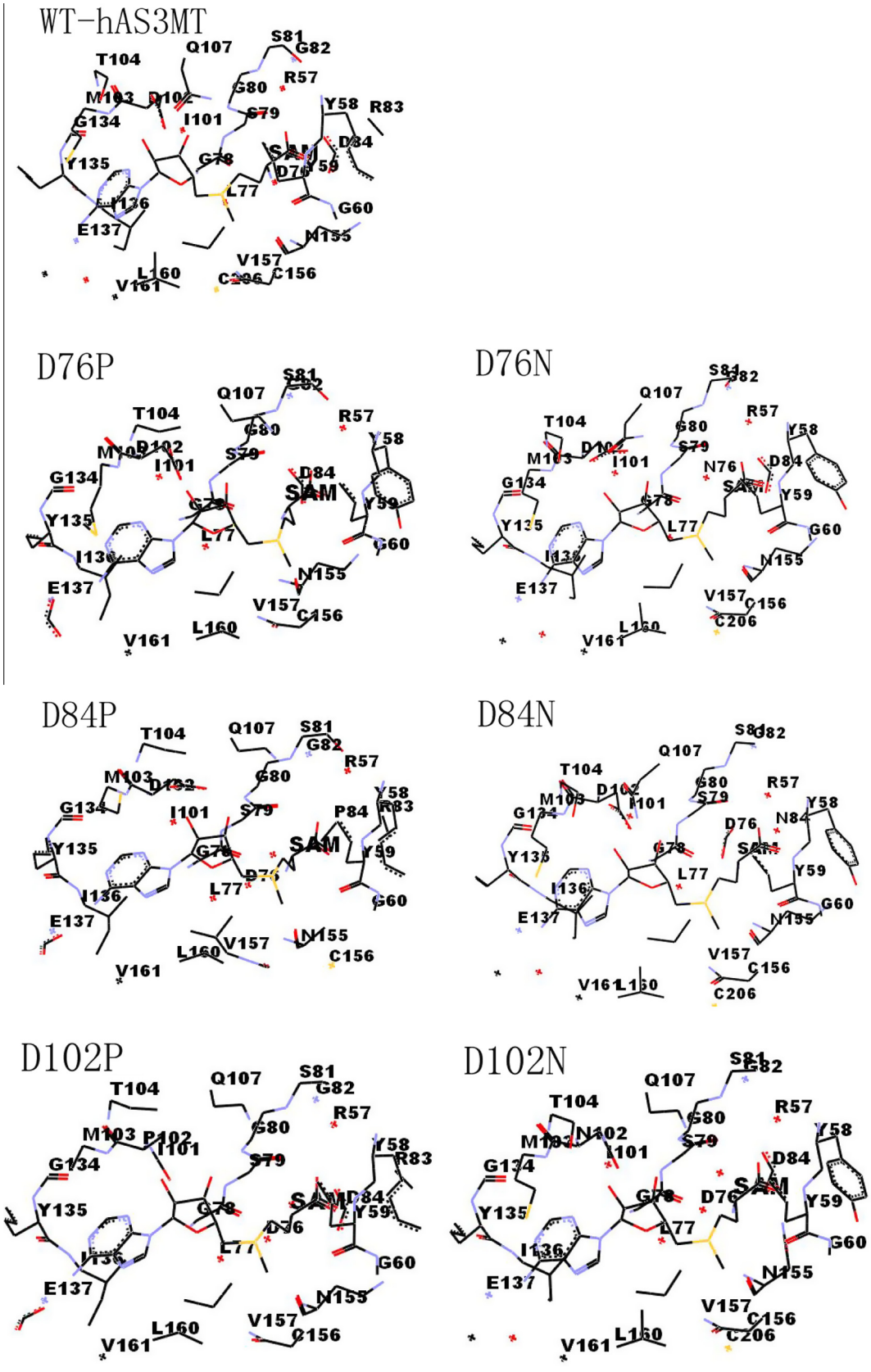

Fig. 7. Interaction mode between SAM, WT-hAS3MT and mutants, only the residues 5.0 Å around SAM are displayed.

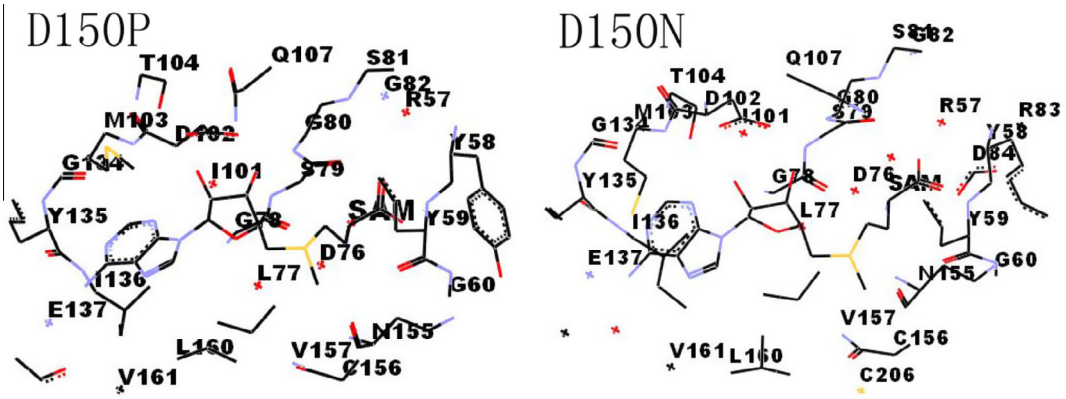

Fig. 7 (*continued*)

Table 5
The residues 5.0 Å around SAM based on the models of WT and the mutants.

	Residues 5.0 Å around SAM
WT	57-RYYG-60,76-DLGSGSGRD-84,101-IDMT-104,Q107,134-GYIE-137,155-NCV-157,160-LV-161, C206
D76P	57-RYYG-60,77-LGSGSG-82,101-IDMT-104,Q107,134-GYIE-137,155-NCV-157,160-LV-161
D76N	57-RYYG-60,76-NLGSGSG-82,D84,101-IDMT-104,Q107,134-GYIE-137,155-NCV-157,160-LV-161, C206
D84P	57-RYYG-60,76-DLGSGSGRP-84,101-IDMT-104,Q107,134-GYIE-137,155-NCV-157,160-LV-161
D84N	57-RYYG-60,76-DLGSGSG-82,N84,101-IDMT-104,Q107,134-GYIE-137,155-NCV-157,160-LV-161,C206
D102P	57-RYYG-60,76-DLGSGSGRD-84,101-IPMT-104, Q107,134-GYIE-137,155-NCV-157,160-LV-161
D102N	57-RYYG-60,76-DLGSGSG-82,D84,101-INMT-104,Q107,134-GYIE-137,155-NCV-157,160-LV-161, C206
D150P	57-RYYG-60,76-DLGSGSGRD-84,101-IDMT-104,Q107,134-GYIE-137,155-NCV-157,160-LV-161
D150N	57-RYYG-60,76-DLGSGSGRD-84,101-IDMT-104,Q107,134-GYIE-137,155-NCV-157,160-LV-161,C206

ment criterion [34], the secondary structure of the mutants was calculated from the integrated areas of the component bands (Table 3B). The secondary structures of the eight mutants utilizing ATR-FTIR were in accordance with those utilizing CD spectra.

3.3. Determinations of SAM dissociation constant for the mutants by fluorescence spectra

Fluorescence quenching is a powerful technique to investigate the binding information between protein and small molecules. To evaluate the interactions between hAS3MT mutants, WT-hAS3MT and SAM, we measured the fluorescence spectra (300–420 nm) of the enzyme. SAM did not emit in the measured range. The dissociation constants k_d estimated for hAS3MT and SAM were calculated from Eq. (3) [22] shown in Fig. 6 and Table 4. The k_d values of these mutants increased by 3.5- to 8.1-fold, suggesting the affinities of these mutants for SAM were 3.5- to 8.1-fold lower than that of the wild-type (WT) protein. The relative k_d value of D150N was consistent with its relative $K_{M(SAM)}$ value.

3.4. The model of WT-hAS3MT and mutants hAS3MT with SAM

The models of hAS3MT (WT and the mutants) were built using modeller9v8. The crystal structure of CmArsM with the cofactor SAM was used as the template. Alignment of the sequences reveals 42% identity between hAS3MT and CmArsM. The models quality was estimated on the basis of a QMEAN scoring function acceptably ranging between 0.60 and 0.65 [33]. The secondary structure arrangement of the hAS3MT model was almost identical to that of the CmArsM structure. The sites in the SAM-binding pocket (5.0 Å around SAM) of WT-hAS3MT and the mutants (D76P, D76N, D84P, D84N, D102P, D102N, D150P and D150N) were displayed in Fig. 7 and Table 5. The SAM model-derived WT-hAS3MT showed that the As-binding sites Cys156 and Cys206 were located in the SAM-binding pocket. However, the As-binding site Cys206 was not located in the SAM-binding pockets of mutants D84P, D102P and D150P. The other residues in the SAM-binding pocket were the same as those in WT. In the mutant D76P, the residues 5 Å around SAM missed the residues P76, L77, R83, D84 and Cys206. The mutants D76N, D84N and D102N only lost the residue R83 in the SAM-binding pocket. The residues in the SAM-binding pocket of D150N were identical with those in WT. The residue 102 and SAM in mutant D102P did not form hydrogen bonds, whereas the residue 102 and –OH of SAM in D102N were prone to forming hydrogen bonds. The distances between the O of carboxyl group in Asp102 and H of ribose hydroxyl in SAM were 2.037 and 2.081 Å, respectively. Therefore, the carboxyl group of Asp102 and ribose hydroxyl groups of SAM formed hydrogen bonds (Fig. 8), which further proved that the ribose hydroxyl group of SAM significantly affect the SAM binding to hAS3MT [35]. The affinity between D102P and SAM turned weakest owing to the disappeared hydrogen bonding. Meanwhile, the residues 5 Å around SAM in mutants D76P, D76N, D84P, D84N, D102P, D102N and D150P were also altered, which suggested that the microenvironment of SAM-binding changed and demonstrates that the binding of SAM to the mutants was weakened.

4. Discussion

There are two pathways to investigate the interaction between cofactor SAM and the SAM-dependent methyltransferase. One is to explore the contributions of each functional group of SAM binding to DNA methyltransferases via testing the analogs of the methyltransferase inhibitor S-adenosylhomocysteine (SAH) for the ability to inhibit methylation by HhaI and HaeIII DNA methyltransferase [35]. Another is to find out the functional residues in methyltransferase relating to the SAM-binding via designing the mutants of the methyltransferase [22,36,37]. The acidic residues in other

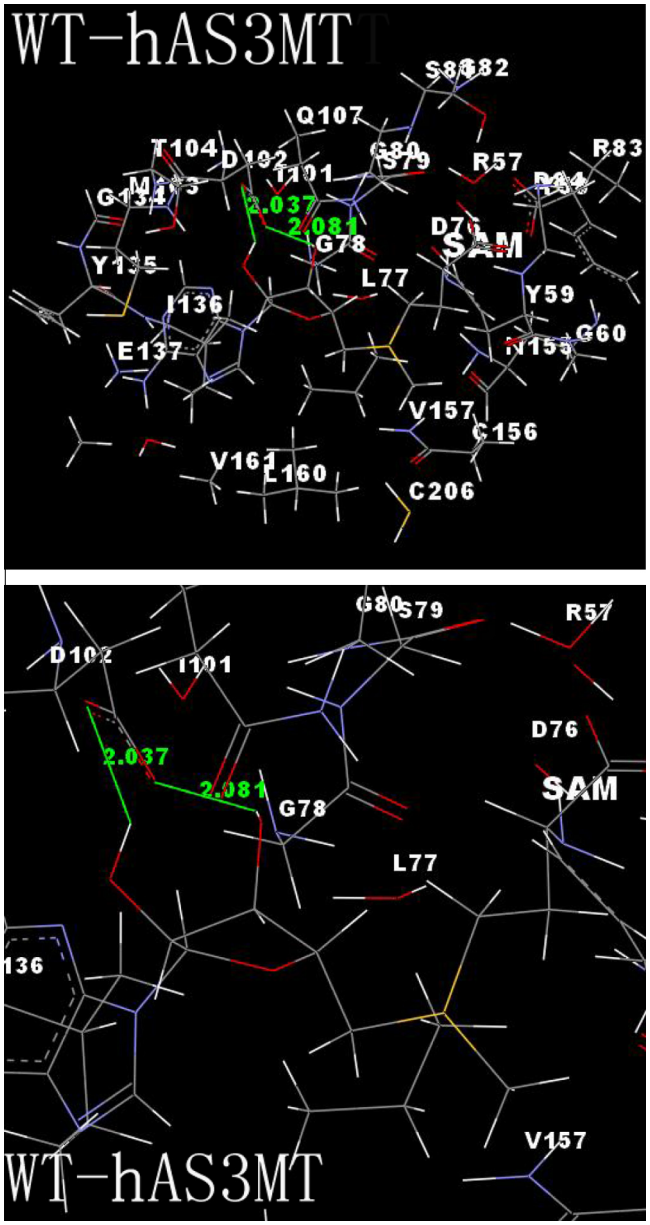

Fig. 8. Interaction mode of WT-hAS3MT with SAM, only the residues 5.0 Å around SAM is displayed. The hydrogen bonds formed between Asp102 of WT-hAS3MT and SAM are all represented by green lines. The length of the hydrogen bonds is also labeled. (B) is part of a larger version of the (A).

methyltransferases have been proved to play important roles in SAM binding via forming hydrogen bonds with SAM directly or through water molecules [18–21]. The residues Asp76, 84,102 and 150 in hAS3MT are conserved and belong to the predicted SAM-binding motifs or near the motif, but the actual function of them have not been studied. Therefore, the functions of the acidic residues D76, D84, D102 and D150 in hAS3MT were studied and the eight mutants D76P, D76N, D84P, D84N, D102P, D102N, D150P and D150N were designed. All the mutants except for D150N abolished the arsenic methylation activities. Nevertheless, the reasons accounting for the hindered methyl group transfer from SAM to arsenic atom in the mutants are still undefined. It has been previously reported that [38–42] the methyl transfer from SAM to an acceptor atom in the SAM-dependent methyltransferase is a S_N2 mechanism requiring some indispensable conditions. Firstly, the methyl donor (SAM) and the methyl acceptor (the substrate) must bind to the enzyme. Secondly, the distance between the S^+-CH_3 and acceptor atom need to be appropriate. Thirdly, the S^+ and C atoms of the S^+-CH_3 in SAM and the methyl acceptor atom should maintain a nearly linear conformation, where the lone pair orbital of the methyl acceptor atom is oriented toward the methyl group C of SAM, preparing the subsequent S_N2 methyl transfer reaction.

The hAS3MT belongs to the Rossmann fold SAM-dependent methyltransferase with the highly conserved glycine-rich sequence of 74-ILDLGSGSG-82 as the hallmark. The substrate of hAS3MT is arsenic with a lone pair orbital and the methyl donor of arsenic methylation is SAM. The methyl transfer from SAM to arsenic in hAS3MT should also conform to the conditions of methyl transfer mentioned above. The CD, ATR-FTIR and the models of the mutants with SAM showed that the enzyme conformation and the microenvironment around SAM were different from those of the WT. As-binding sites Cys156 and Cys206 were located in the SAM-binding pocket of WT-hAS3MT. In contrast, the models of mutants D76P, D84P, D102P and D150P exhibit that no As-binding site Cys206 was discerned in the range 5 Å around SAM. The arsenic and the methyl group C of SAM in mutants D76P, D84P, D102P and D150P were more distantly spaced than those in WT, which did not favor the methyl group transfer from SAM to arsenic. The dissociation constant k_d values verify that SAM bound to the mutants more weakly than WT, which also probably influenced the methyl transfer process. The mutants D76N, D84N and D102N missed the R83 in SAM-binding pocket, which probably was the reason for the three mutants lost their catalytic activity. Therefore, all the mutants D76P, D76N, D84P, D84N, D102P, D102N and D150P except for D150N were deprived of arsenic methylation activities completely. So we concluded that the residues Asp102 in motif II formed hydrogen bonds with the ribose hydroxyl groups of SAM and the length of the hydrogen bond were 2.037 and 2.081, respectively, Asp76 and 84 in motif I or near motif I, which were located in the SAM-binding pocket, greatly impacted the SAM-binding. The residue Asp150 also influenced the catalytic activity of the hAS3MT via affecting the SAM bind to hAS3MT. All the residues Asp76, 84, 102 and 150, especially the residue Asp102, impacted the SAM-binding pocket and the catalytic activity of hAS3MT.

Acknowledgements

This work is supported by the National Basic Research Program of China (2013CB922102) and the National Natural Science Foundation of China (21075064, 21027013, 21021062, 21275072 and 21201101).

References

[1] Kozbial, P.Z. and Mushegian, A.R. (2005) Natural history of S-adenosylmethionine-binding proteins. BMC Struct. Biol. 5, 1–26.
[2] Fontecave, M., Atta, M. and Mulliez, E. (2004) S-adenosylmethionine: nothing goes to waste. Trends Biochem. Sci. 29, 243–249.
[3] Roje, S. (2006) S-Adenosyl-L-methionine: beyond the universal methyl group donor. Phytochemistry 67, 1686–1698.
[4] Thomas, D.J., Waters, S.B. and Stýblo, M. (2004) Elucidating the pathway for arsenic methylation. Toxicol. Appl. Pharmacol. 198, 319–326.
[5] Wuosmaa, A.M. and Hager, L.P. (1990) Methyl chloride transferase: a carbocation route for biosynthesis of halometabolites. Science 249, 160–162.
[6] Saxena, D., Aouad, S., Attieh, J. and Saini, H.S. (1998) Biochemical characterization of chloromethane emission from the wood-rotting fungus *Phellinus pomaceus*. Appl. Environ. Microb. 64, 2831–2835.
[7] Anantharaman, V., Koonin, E.V. and Aravind, L. (2002) Comparative genomics and evolution of proteins involved in RNA metabolism. Nucleic Acids Res. 30, 1427–1464.
[8] Aposhian, H.V. (1997) Enzymatic methylation of arsenic species and other new approaches to arsenic toxicity. Annu. Rev. Pharmacol. Toxicol. 37, 397–419.
[9] Hayakawa, T., Kobayashi, Y., Cui, X. and Hirano, S. (2005) A new metabolic pathway of arsenite: arsenic–glutathione complexes are substrates for human arsenic methyltransferase Cyt19. Arch. Toxicol. 79, 183–191.

[10] Lin, S., Shi, Q., Nix, F.B., Styblo, M., Beck, M.A., Herbin-Davis, K.M., Hall, L.L., Simeonsson, J.B. and Thomas, D.J. (2002) A novel S-adenosyl-L-methionine: arsenic(III) methyltransferase from rat liver cytosol. J. Biol. Chem. 277, 10795–10803.
[11] Wang, S.P., Li, X.L., Song, X.L., Geng, Z.R., Hu, X. and Wang, Z.L. (2012) Rapid-equilibrium kinetic analysis of arsenite methylation catalyzed by recombinant human arsenic (+3 oxidation state) methyltransferase (hAS3MT). J. Biol. Chem. 287, 38790–38799.
[12] Waters, S.B., Devesa, V., Luz, M.D.R., Styblo, M. and Thomas, D.J. (2004) Endogenous reductants support the catalytic function of recombinant rat Cyt19, an arsenic methyltransferase. Chem. Res. Toxicol. 17, 404–409.
[13] Fomenko, D.E., Xing, W.B., Adair, B.M., Thomas, D.J. and Gladyshev, V.N. (2007) High-throughput identification of catalytic redox-active cysteine residues. Science 315, 387–389.
[14] Li, J.X., Waters, S.B., Drobna, Z., Devesa, V., Styblo, M. and Thomas, D.J. (2005) Arsenic (+3 oxidation state) methyltransferase and the inorganic arsenic methylation phenotype. Toxicol. Appl. Pharmacol. 204, 164–169.
[15] Song, X.L., Geng, Z.R., Zhu, J.S., Li, C.Y., Hu, X., Bian, N.S., Zhang, X.R. and Wang, Z.L. (2009) Structure–function roles of four cysteine residues in the human arsenic (+3 oxidation state) methyltransferase (hAS3MT) by site-directed mutagenesis. Chem. Biol. Interact. 179, 321–328.
[16] Kagan, R.M. and Clarke, S. (1994) Widespread occurrence of three sequence motifs in diverse S-adenosylmethionine-dependent methyltransferases suggests a common structure for these enzymes. Arch. Biochem. Biophys. 310, 417–427.
[17] Thomas, D.J., Li, J.X., Waters, S.B., Xing, W.B., Adair, B.M., Drobna, Z., Devesa, V. and Stýblo, M. (2007) Arsenic (+3 oxidation state) methyltransferase and the methylation of arsenicals. Exp. Biol. Med. 232, 3–13.
[18] Bugl, H., Fauman, E.B., Staker, B.L., Zheng, F., Kushner, S.R., Saper, M.A., Bardwell, J.C. and Jakob, U. (2000) RNA methylation under heat shock control. Mol. Cell 6, 349–360.
[19] Feder, M., Pas, J., Wyrwicz, L.S. and Bujnicki, J.M. (2003) Molecular phylogenetics of the RrmJ/fibrillarin superfamily of ribose 2′-O-methyltransferases. Gene 302, 129–138.
[20] Schwer, B., Saha, N., Mao, X.D., Chen, H.W. and Shuman, S. (2000) Structure-function analysis of yeast mRNA cap methyltransferase and high-copy suppression of conditional mutants by adomet synthase and the ubiquitin conjugating enzyme Cdc34p. Genetics 155, 1561–1576.
[21] Ajees, A.A., Marapakala, K., Packianathan, C., Sankaran, B. and Rosen, B.P. (2012) Structure of an As(III) S-adenosylmethionine methyltransferase: insights into the mechanism of arsenic biotransformation. Biochemistry 51, 5476–5485.
[22] Sankpal, U.T. and Rao, D.N. (2002) Mutational analysis of conserved residues in HhaI DNA methyltransferase. Nucleic Acids Res. 30, 2628–2638.
[23] Kuroki, T. and Matsushima, T. (1987) Performance of short-term tests for detection of human carcinogens. Mutagenesis 2, 33–37.
[24] Geng, Z.R., Song, X.L., Xing, Z., Geng, J.L., Zhang, S.C., Zhang, X.R. and Wang, Z.L. (2009) Effects of selenium on the structure and function of recombinant human S-adenosyl-L-methionine dependent arsenic (+3 oxidation state) methyltransferase in *E. coli*. J. Biol. Inorg. Chem. 14, 485–496.
[25] Sanger, F., Nicklen, S. and Coulson, A.R. (1977) DNA sequencing with chain-terminating inhibitors. Proc. Natl. Acad. Sci. USA 7, 5463–5467.
[26] Bradford, M.M. (1976) A rapid and sensitive method for the quantitation of microgram quantities of protein utilizing the principle of protein-dye binding. Anal. Biochem. 72, 248–254.
[27] Le, X.C., Lu, X.F. and Li, X.F. (2004) Arsenic speciation. Anal. Chem. 76, 27A–33A.
[28] Walton, F.S., Waters, S.B., Jolley, S.L., LeCluyse, E.L., Thomas, D.J. and Styblo, M. (2003) Selenium compounds modulate the activity of recombinant rat As(III) methyltransferase and the methylation of arsenite by rat and human hepatocytes. Chem. Res. Toxicol. 16, 261–265.
[29] Yang, J.T., Wu, C.S.C. and Martinez, H.M. (1986) Calculation of protein conformation from circular dichroism. Methods Enzymol. 130, 208–269.
[30] Byler, D.M., Brouillette, J.N. and Susi, H. (1986) Quantitative studies of protein structure by FTIR spectral deconvolution and curve fitting. Spectroscopy 3, 29–32.
[31] Li, D.J., Zhu, J.F., Jin, J. and Yao, X.J. (2007) Studies on the binding of nevadensin to human serum albumin by molecular spectroscopy and modeling. J. Mol. Struct. 846, 34–41.
[32] Benkert, P., Tosatto, S.C.E. and Schomburg, D. (2008) QMEAN: a comprehensive scoring function for model quality assessment. Proteins 71, 261–277.
[33] Song, X.L., Geng, Z.R., Li, X.L., Hu, X., Bian, N.S., Zhang, X.R. and Wang, Z.L. (2010) New insights into the mechanism of arsenite methylation with the recombinant human arsenic (+3) methyltransferase (hAS3MT). Biochimie 92, 1397–1406.
[34] Surewicz, W.K. and Mantsch, H.H. (1988) New insight into protein secondary structure from resolution-enhanced infrared-spectra. Biochim. Biophys. Acta 952, 115–130.
[35] Cohen, H.M., Griffiths, A.D., Tawfik, D.S. and Loakes, D. (2005) Determinants of cofactor binding to DNA methyltransferases: insights from a systematic series of structural variants of S-adenosylhomocysteine. Org. Biomol. Chem. 3, 152–161.
[36] Takata, Y., Konishi, K., Gomi, T. and Fujioka, M. (1994) Rat guanidinoacetate methyltransferase. J. Biol. Chem. 269, 5537–5542.
[37] Hamahata, A., Takata, Y., Gomi, T. and Fujioka, M. (1996) Probing the S-adenosylmethionine-binding site of rat guanidinoacetate methyltransferase. Biochem. J. 317, 141–145.
[38] Velichkova, P. and Himo, F. (2006) Theoretical study of the methyl transfer in guanidinoacetate methyltransferase. J. Phys. Chem. B 110, 16–19.
[39] Kuhn, B. and Kollman, P.A. (2000) QM-FE and molecular dynamics calculations on catechol O-methyltransferase: free energy of activation in the enzyme and in aqueous solution and regioselectivity of the enzyme-catalyzed reaction. J. Am. Chem. Soc. 122, 2586–2596.
[40] Wu, R.B. and Cao, Z.X. (2008) QM/MM study of catalytic methyl transfer by the N5-glutamine SAM-dependent methyltransferase and its inhibition by the nitrogen analogue of coenzyme. J. Comput. Chem. 29, 350–357.
[41] Roca, M., Andreś, J., Moliner, V., Tunõń, I. and Bertrán, J. (2005) On the nature of the transition state in catechol O-methyltransferase. A complementary study based on molecular dynamics and potential energy surface explorations. J. Am. Chem. Soc. 127, 10648–10655.
[42] Velichkova, P. and Himo, F. (2005) Methyl transfer in glycine N-methyltransferase. A theoretical study. J. Phys. Chem. B 109, 8216–8219.